

# Projected climate-driven changes of water table depth in the world's major groundwater basins

Maya Costantini<sup>1</sup>, Jeanne Colin<sup>1</sup>, Bertrand Decharme<sup>1</sup>

<sup>1</sup>Centre National de Recherches Météorologiques (CNRM), Météo-France/CNRS, Toulouse, France

## Key Points:

- The impact of climate change on water table depth in the world's major groundwater basins is assessed using CMIP6 global simulations.
- Projections run with four SSP scenarios show a global rising of groundwater by 2100, with the occurrence of a depletion in numerous regions.
- In 2100, 31% to 43% of the world's population could face water scarcity issues or flood risks worsened by these water table depth changes.

---

Corresponding author: Maya Costantini, [maya.costantini@meteo.fr](mailto:maya.costantini@meteo.fr)

## 12 Abstract

13 As groundwater found in aquifers is the main reservoir of freshwater for human activ-  
14 ity, knowledge of the future response of groundwater to climate change is key for improving  
15 water management adaptation plans. We analyse the climate-driven evolution of future  
16 levels of unconfined aquifers in the 218 world's major groundwater basins in global climate  
17 simulations following the latest IPCC scenarios, run with models able to capture feedbacks  
18 among climate, land use and groundwater. We find a rising of groundwater levels on global  
19 average, which is consistent with the projected global intensification of precipitation. This  
20 signal presents large regional disparities which mostly match the patterns of precipitation  
21 changes. As the climate models we used do not simulate human groundwater withdrawals  
22 (irrigation as well as domestic and industrial uses) which represent the other main driver  
23 of groundwater levels evolution, we also use FAO maps of present-day irrigated areas and  
24 projections of population in 2100 to identify regions where groundwater withdrawals could  
25 exacerbate the projected depletion, or even reverse a projected rise into a depletion. De-  
26 pending on the scenario, we then find a rise (respectively a depletion) of groundwater levels  
27 in 2100 over 33[28-39]% to 42[41-45]% (respectively 26[25-32]% to 37[36-40]%) of the area  
28 covered by the 218 world's major groundwater basins. And we estimate that 31[29-36]% to  
29 43[42-44]% of the world's population could be affected by these groundwater changes, facing  
30 either water scarcity issues (for 29[27-33]% to 40[39-40]% of the population), or increased  
31 risks of flooding (for 1.7[1.5-2.2]% to 2.2[2.2-2.4]% of the population).

## 32 1 Introduction

33 Groundwater, stored in permeable geological structures (aquifers), constitutes the largest  
34 unfrozen reserve of freshwater on Earth. It amounts to approximately 35% of human fresh  
35 water withdrawals (Doll et al., 2012) and sustains ecosystems by supplying baseflow during  
36 dry periods. The recharge of aquifers stems mainly from rainfall, melted snow, and water  
37 exchanges with inland water bodies. Conversely, groundwater sustains these bodies of water  
38 and is the main driver of river flow. To a lesser extent, it also contributes to evapotran-  
39 spiration in groundwater-dependent ecosystems. In addition to these natural water fluxes,  
40 pumping and soil infiltration of irrigation water also affect groundwater levels. The evolu-  
41 tion of groundwater resources with climate change is therefore of great importance for both  
42 humankind and natural ecosystems.

43 As climate change modify the natural hydrological cycle as well as human water use and  
44 demand, it also affect groundwater resources (Green et al., 2011; R. G. Taylor et al., 2013;  
45 Wada, 2016; Scanlon et al., 2012; IPCC, 2021c). Over the past decade, studies exploring the  
46 impact of future climate change on groundwater have relied on hydrological models driven  
47 by atmospheric forcing or estimated recharge. Until the recent work of Wu et al. (2020), who  
48 used a fully coupled global climate model, studies exploring the impacts of future climate  
49 change on groundwater have relied on hydrological models driven by atmospheric forcings  
50 or estimated recharges. Few of these studies are global (Wada et al., 2012; Reinecke et al.,  
51 2021). In most cases, the spatial scale is limited to a given set of watershed or a single region  
52 (Meixner et al., 2016; Maxwell & Kollet, 2008; Condon et al., 2020; Amanambu et al., 2020).  
53 These global and regional studies give valuable insights regarding the future of groundwater  
54 resources, but regardless of their scale, they can not take into account the groundwater-  
55 climate feedbacks because of their modelling framework. A number of studies have shown  
56 that including groundwater in a coupled surface-atmosphere model leads to an increase  
57 of evapotranspiration, which can impact near-surface temperature and precipitation (e.g.  
58 Anyah et al. (2008); Larsen et al. (2016); Wang et al. (2018)). Without these feedbacks,  
59 the response of groundwater to climate change may be biased (Maxwell & Kollet, 2008;  
60 Meixner et al., 2016), and the future long-term evolution of the land surface hydrology can  
61 be misleading (Boe, 2021).

62 Over the past few years, a number of authors have recommended the inclusion of a  
63 representation of groundwater in Earth system models and global climate models (Clark  
64 et al., 2015; Fan et al., 2019; Boe, 2021; Gleeson et al., 2021), and some of them have  
65 argued that these integrated models would ultimately help to assess the future effects of  
66 climate change on groundwater (Fan et al., 2019; Gleeson et al., 2021). Taking up this  
67 suggestion, Wu et al. (2020) considered an ensemble of future global simulations following  
68 the old business-as-usual RCP8.5 scenario (designed for the fifth phase of the Coupled  
69 Model Intercomparison Project CMIP5 (K. E. Taylor et al., 2012)), performed with the  
70 Community Earth System Model version 4.0 (Kay et al., 2015) which includes a simple  
71 parameterization of aquifers. The authors analysed the future evolution of groundwater  
72 storage in this ensemble of projections, but they limited their assessment to 7 key mid-  
73 latitudes aquifers, thus failing to provide a worldwide picture of the global changes.

74 In this present study, we look to go beyond the work of Wu et al. (2020) by providing  
75 a wider scale analysis of future groundwater levels using more recent global climate simu-  
76 lations. To do so, we consider the future evolution of the 218 world's major groundwater  
77 basins which cover 43% of the global land surface (without Antarctica and Greenland) and  
78 under four of the up-to-date greenhouse gas concentration pathways scenarios (SSP126,  
79 SSP245, SSP370 and SSP585) (O'Neill et al., 2017). The simulations were performed at  
80 the French National Center for Meteorological Research (CNRM in french), for the sixth  
81 phase of the Coupled Model Intercomparison Project (CMIP6) (Eyring et al., 2016) with our  
82 two fully coupled climate models CNRM-CM6-1 (Voltaire et al., 2019) and CNRM-ESM2-1  
83 (Seferian et al., 2019). Both models include a hydrogeological representation of unconfined  
84 aquifer processes in the world's major groundwater basins (Decharme et al., 2019; Vergnes  
85 & Decharme, 2012). They simulate the evolution of the Water Table Depth (WTD), de-  
86 fined as the depth of the piezometric head in each aquifer, using a two-dimensional diffusive  
87 scheme of the groundwater flows also accounting for two-way water exchanges with the river  
88 and the unsaturated soil column. This two-way coupling allows the CNRM models to cap-  
89 ture groundwater-climate feedbacks, and CNRM-ESM2-1 also accounts for land-use changes  
90 feedbacks.

91 The recently issued IPCC Sixth Assessment Report (AR6) (IPCC, 2022a) pointed out  
92 the necessity to include such feedbacks in projections of future groundwater resources. With  
93 the inclusion of these processes in the CNRM models, the present study contributes to  
94 further narrow one of the knowledge gaps identified in the AR6 (IPCC, 2022a). However,  
95 human groundwater withdrawals (irrigation as well as domestic and industrial uses), which  
96 constitute an important driver of WTD evolution (Rodell et al., 2009; Panda et al., 2021;  
97 Scanlon et al., 2012; Doll et al., 2012; Jasechko & Perrone, 2021; de Graaf et al., 2019), are  
98 not simulated in the CNRM models, as is also the case for most of the models used in the  
99 previously mentioned studies and all of those using global fully coupled models. Therefore,  
100 our models results only account for the "natural" part of the climate change-induced changes  
101 of water table depths, we will refer to as their "climate-driven" evolution.

102 Hereafter, the evolution of WTD is analysed over the 1850-2100 period using CMIP6  
103 simulations run with the CNRM models. The results are put in perspective with a multi-  
104 model analysis of the precipitation and evapotranspiration changes simulated by 18 other  
105 state-of-the-art global climate models which contributed to CMIP6. Finally, we discuss the  
106 foreseeable impacts of the projected evolution of groundwater levels on the human water  
107 need in 2100, and vice versa.

## 108 2 Materials and Methods

### 109 2.1 CNRM models

110 The global climate model CNRM-CM6-1 (<http://www.umr-cnrm.fr/cmip6/spip.php?article11>) and the Earth system model CNRM-ESM2-1 (<http://www.umr-cnrm.fr/cmip6/spip.php?article10>) are both two global fully coupled atmosphere-ocean-surface  
111 general circulation models of the CNRM. They are part of the models engaged in CMIP6  
112 to contribute to the AR6 (Eyring et al., 2016; IPCC, 2021a). These models are run at  
113 a resolution of approximately  $1.5^\circ$  and based on the same core of components. CNRM-  
114 CM6-1 simulates the main physical processes in the ocean, the sea ice, the land surface  
115 and the atmosphere (Voldoire et al., 2019). Using the same physics, CNRM-ESM2-1 repre-  
116 sents in addition the global carbon cycle including carbon cycling in vegetation. Leaf level  
117 photosynthesis, plant respiration, stomatal conductance, and plant biomass are explicitly  
118 computed by the model. Leaf phenology results directly from the simulated carbon bal-  
119 ance of the canopy (Delire et al., 2020). This allows to represent the physiological effects  
120 of  $\text{CO}_2$  on plant transpiration and growth (increased water use efficiency and fertilisation  
121 effect). CNRM-ESM2-1 also accounts for land-use-land-cover change scenarios derived from  
122 the Land Use Harmonized version 2 release LUH2 (Hurtt et al., 2020) for CMIP6 and in-  
123 cludes an interactive atmospheric chemistry scheme and an interactive tropospheric aerosols  
124 scheme (Seferian et al., 2019).  
125  
126

127 In these two climate models, the ISBA-CTRIP (Decharme et al., 2019) (Interaction-  
128 Soil-Biosphere-Atmosphere - CNRM version of the Total Runoff Integrating Pathways) land  
129 surface system provides a physical and realistic representation of the continental hydrolog-  
130 y (<http://www.umr-cnrm.fr/spip.php?article1092&lang=en>). ISBA uses multilayer  
131 schemes for both the soil and the snowpack to calculate the time evolution of the water  
132 and energy budgets at the land surface and to provide water flow to CTRIP. In this way,  
133 CTRIP which simulates inundation dynamic, groundwater processes and river discharges in  
134 the ocean. Because of the coarse resolution of the model ( $0.5^\circ$ ), only the 218 world's largest  
135 unconfined aquifer basins with diffusive groundwater movements are represented for the mo-  
136 ment (Vergnes & Decharme, 2012; Vergnes et al., 2012). More complex aquifer systems like  
137 confined, karstic, orogenic and localized shallow aquifers remain difficult to simulate at the  
138 global scale due to the lack of precise global parameter database. The hydrogeological mod-  
139 elling of groundwater dynamics relies on a two-dimensional one-layer diffusive widespread  
140 unconfined aquifer scheme (Vergnes et al., 2012) based on the well-known MODCOU hy-  
141 drogeological model (Vergnes, May 2014; Ledoux et al., 1989). This scheme computes the  
142 WTD in aquifers according to the lateral groundwater fluxes, the two-way water exchanges  
143 with the rivers (Vergnes & Decharme, 2012; Vergnes et al., 2012) and the unsaturated soil  
144 (Decharme et al., 2019; Vergnes J.P., Decharme B, 2014). In ISBA-CTRIP, the soil water  
145 used for transpiration is withdrawn throughout the soil according to a vertical root-density  
146 profile allowing interaction between WTD and roots, as long as WTD is not too deep. The  
147 rooting depth reaches 1.5m for low vegetation (crop, grassland, etc.), 4m and 3m for temper-  
148 ate and boreal forests, and 8m for tropical forests (see Table 1 and Fig.2.C in Decharme et al.  
149 (2019). Groundwater basins boundaries and their hydrogeological parameters were estimated  
150 using global maps of groundwater resources and topological, lithological and geological data  
151 sets (Vergnes & Decharme, 2012). Groundwater basins have been delimited using the global  
152 map of the groundwater resources of the world from the Worldwide Hydrogeological Map-  
153 ping and Assessment Programme (WHYMAP), the hydrogeological map over the United  
154 States from the U.S. Geological Survey (USGS) and the global map of lithology (Durr et  
155 al., 2005). This last map also allows one to determine the transmissivity and the effective  
156 porosity in each aquifer basin (Vergnes & Decharme, 2012; Decharme et al., 2019).

157 Groundwater processes as well as other hydrological features were validated thoroughly  
158 during the last decade in ISBA-CTRIP on a regional and global scale. These evaluations  
159 were performed specifically by comparing model results to in-situ measurements of the  
160 piezometric head, the GRACE terrestrial water storage estimates and a large set of in-situ  
161 river discharges measurements in forced land surface applications (Decharme et al., 2019;  
162 Vergnes & Decharme, 2012; Vergnes et al., 2012; Vergnes J.P., Decharme B, 2014) as well as

163 in our fully-coupled climate models (Voldoire et al., 2019; Roehrig et al., 2020). Finally, it  
 164 was thanks to this evaluation work that the ISBA-CTRIP land surface system was used in  
 165 many global hydrological applications, some of which highlight important results regarding  
 166 global hydrology and climate change (Padron et al., 2020; Cazenave et al., 2014; Douville  
 167 et al., 2013).

168 In this study, we only consider the WTD which are shallower than 100 *m* ( $WTD < 100m$ )  
 169 over 1985 – 2014 in the historical CMIP6 experiment (present-day climate). In deeper  
 170 aquifers, we assume that groundwater is too disconnected from the surface to be significantly  
 171 impacted by climate change at the time scales we consider (less than 250 years). This is  
 172 especially true over hyper-arid regions (e.g. in the Sahara desert) where fossil aquifers were  
 173 recharged by precipitation during paleoclimatic periods (R. G. Taylor et al., 2013; Scanlon  
 174 et al., 2006; Alley et al., 2002). The current annual precipitation rates here are extremely  
 175 weak, which limits the groundwater recharge and thus constrains WTD to very deep levels.

## 176 2.2 CMIP6 Experiments and Data Post-processing

177 Our analysis of the water table depth changes is based on the results of CMIP6 sim-  
 178 ulations run with the CNRM models. The multi-model analysis includes the results of  
 179 CMIP6 simulations run with the 18 models of the CMIP6 panel which had published the  
 180 variables of interest (see next subsection) at the time of our analysis (see Table 1). For the  
 181 past and present-day climate (1850 – 2014) we use simulations run for the historical exper-  
 182 iment, which is part of the CMIP6 core experiments (Eyring et al., 2016). For the future  
 183 period (2015 – 2100), we use simulations run for the ScenarioMIP experiments (O’Neill et  
 184 al., 2016, 2017; Meinshausen et al., 2017). We consider four scenarios, based on different  
 185 Shared Socioeconomic Pathways (SSP) and different levels of radiative forcing (increase of  
 186 the atmosphere’s radiative balance (in  $W.m^{-2}$ ) between 1850 and 2100) : SSP126, SSP145,  
 187 SSP370, SSP585. To put it simply, the SSP126 scenario is the optimistic one. It is defined  
 188 by a sustainable societal development, with a relatively low radiative forcing. The SSP245  
 189 scenario is a middle-of-the-road pathway. It depicts a world where the socioeconomic trends  
 190 do not deviate too much from the historical period patterns, with an intermediate radiative  
 191 forcing. The SSP370 scenario displays regional rivalries and a higher radiative forcing. The  
 192 SSP585 scenario in the worst case scenario, with a strong fossil-fueled development and a  
 193 subsequently high radiative forcing.

194 For each experiment (historical or scenarios), models run an ensemble of simulations,  
 195 composed of several members. These ensembles allows to sample the climate internal vari-  
 196 ability and thus provides a better assessment the models’ response to the evolution of climate  
 197 forcings (the more members, the better). We used all the available members at the time  
 198 of our analysis (see Table 1). The variables we considered are the Water Table Depth  
 199 (*WTD*), precipitation (*PR*) and evapotranspiration (*EVSPSBL*). As the two CNRM cli-  
 200 mate models provide similar results for the variables of interest, their data were processed  
 201 jointly. The same weight was given to CNRM-CM6-1 and CNRM-ESM2-1 by first com-  
 202 puting the ensemble mean of each model (average of all members) for each variable and  
 203 each experiment, and then averaging the two ensemble means. For the multi-model anal-  
 204 ysis of the 18 other state-of-the-art CMIP6 models we considered, we also computed the  
 205 ensemble means of each model, and then we averaged these ensemble means. All the vari-  
 206 ables computed by the different CMIP6 models were regridded on the 0.5° regular grid  
 207 over which WTD is computed in the CNRM models. The interpolation was done us-  
 208 ing a first order conservative remapping provided by the Climate Data Operator (CDO:  
 209 <http://www.idris.fr/media/ada/cdo.pdf>). The interpolation was performed on the en-  
 210 semble means of each model, as were any further statistical computations (time series,  
 211 averages over time periods, percentages of change, etc.).

**Table 1.** Models used and number of members for each model

Global Climate Model	Number of members (historical)	Number of members (SSPs)
<i>CNRM/CNRM – CM6 – 1</i>	30	6
<i>CNRM/CNRM – EMS2 – 1</i>	11	5
<i>BCC/BCC – CSM2 – MR</i>	3	1
<i>CAS/FGOALS – f3 – L</i>	3	3
<i>CAS/FGOALS – g3</i>	6	4
<i>CCCma/CanESM5 – CanOE</i>	3	3
<i>CCCma/CanESM5</i>	40	25
<i>CSIRO/ACCESS – ESM1 – 5</i>	10	3
<i>INM/INM – CM4 – 8</i>	1	1
<i>INM/INM – CM5 – 0</i>	10	1
<i>IPSL/IPSL – CM6A – LR</i>	32	6
<i>MIROC/MIROC6</i>	50	50
<i>MIROC/MIROC – ES2L</i>	10	1
<i>MOHC/UKESM1 – 0 – LL</i>	11	5
<i>NASA – GISS/GISS – E2 – 1 – G</i>	10	1
<i>NCAR/CESM2</i>	11	5
<i>NCAR/CESM2 – WACCM</i>	3	5
<i>NIMS – KMA/KAGE – 1 – 0 – G</i>	3	3
<i>NOAA – GFDL/GFDL – ESM4</i>	2	1
<i>UA/MCM – UA – 1 – 0</i>	1	1

212 The statistical significance of field differences on maps computed using the False De-  
213 tection Rate (FDR) test (Wilks, 2006, 2016). The FDR test is based on a Student test  
214 for the computation of P-values at each grid point. To determine the significance, P-values  
215 are compared to a threshold which depends on the series of P-values (for every grid point).  
216 This test allows to reduce the rate of false significance, which can be rather high for auto-  
217 correlated fields such as climate variables (Wilks, 2006, 2016). In our case, it gives a better  
218 confidence on the fact that the changes we analyze are truly due to climate change rather  
219 than stemming from internal variability. In addition, to provide confidence intervals on the  
220 fraction of surface impacted by significant changes of water table depth, we used a bootstrap  
221 method. We performed a resampling of the 11 members for each scenario and for the 41 his-  
222 torical members. The FDR test of significance was then computed for each of the bootstrap  
223 1000 samples. The confidence intervals we provide correspond to the 5<sup>th</sup> and 95<sup>th</sup> quantiles  
224 of the distribution we obtain with the bootstrap resampling, noted [5<sup>th</sup>-95<sup>th</sup>] hereafter.

### 225 2.3 Future Population Density Projections

226 The evolution of population density (people per km<sup>2</sup>) is derived from the projection  
227 of population density by countries (KC & Lutz, 2017) conducted for CMIP6 and with the  
228 population density in 2015 at 0.5° provided by the SocioEconomic Data and Applications  
229 Center (SEDAC, 2018). For each country, the percentage of change in population density is  
230 computed between 2015 (see Supporting Information Fig.S1) and 2100 according to CMIP6  
231 projections for each SSP scenario (see Supporting Information Fig.S2). This percentage is  
232 then applied to the population density at 0.5° in 2015 provided by the SEDAC. These global  
233 maps of the world's population in 2100 are used to discuss the possible human impacts of  
234 the projected WTD changes. This information is also used to determine in which regions  
235 our results on WTD changes are likely to be biased by the lack of human groundwater  
236 withdrawals in the CNRM models, and in which way this supposed bias might affect our  
237 results. Indeed, groundwater pumping can significantly deplete groundwater in regions with

238 high water requirements for industrial, domestic and agricultural uses (mainly for irrigation  
 239 which represents 70% of groundwater withdrawals (Siebert et al., 2010).)  
 240

## 241 2.4 Present-day Irrigation Data

242 Part of the analysis of our results also refers to maps of areas currently equipped  
 243 for irrigation in each of the CNRM models grid cells. These data, along with those of  
 244 future population density, are used to discuss the influence of groundwater withdrawals  
 245 on our results. They are derived from Siebert et al. (2010) using the FAO (Food and  
 246 Agriculture Organization of the United Nations) data. The two global maps we used provide  
 247 the percentage of areas equipped for irrigation and the percentage of irrigated areas serviced  
 248 by groundwater, at a resolution of 5 arc minutes. The two FAO maps was simply interpolated  
 249 at the  $0.5^\circ$  resolution over which *WTD* is computed in the CNRM models. And we combined  
 250 these two maps to compute the percentages of area equipped for groundwater.

## 251 3 Results

### 252 3.1 Current status and projected groundwater levels

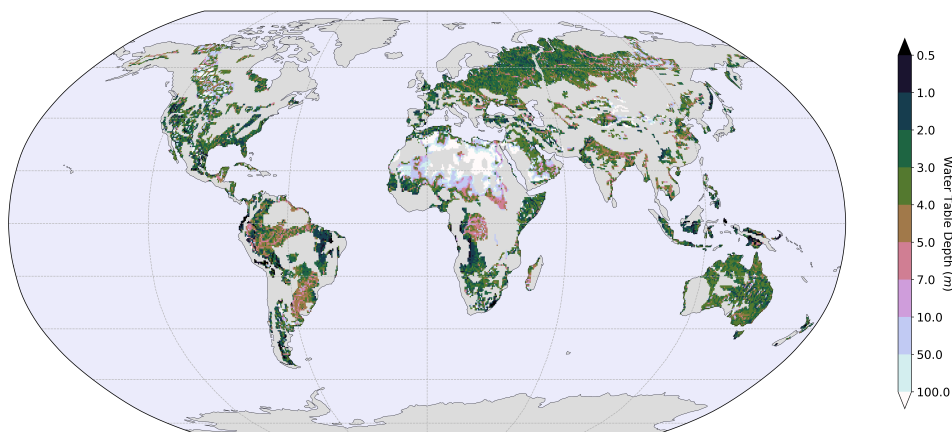


**Figure 1.** Global distribution of the mean WTD simulated by the CNRM global climate models in the 218 world's major groundwater basins over the present-day period (1985 – 2014) in the historical experiment.

253 The current status of the world's major groundwater basins simulated by the CNRM  
 254 models is shown in Fig.1. 40% of the global land area presents a WTD which is shallower  
 255 than 100 *m* and 36% of the land area presents WTD between 1 and 10 *m*. This is consistent  
 256 with estimates from the high resolution observation-driven model of Fan et al. (2013) based  
 257 on observations made over the last 60 years (see Supplementary Material in Fan et al.  
 258 (2013)), where around 38% of the WTD are comprised between 1 and 10 *m*).

259 In agreement with recent observational studies (IPCC, 2021b), the globally yearly averaged  
 260 climate-driven WTD simulated by the CNRM models shows a slight rise over the  
 261 1960 to 2014 period in the historical experiment (Fig.2.A). Following our model estimates,

262 global WTD should continue to rise with climate change in all future scenarios, at least  
 263 until 2100 (i.e. the end of the scenarios). The higher the radiative forcing associated to  
 264 SSP scenarios, the stronger the trend of WTD. The AR6 indicates that the global mean  
 265 annual precipitation over land is also projected to increase until 2100, in all scenarios (IPCC,  
 266 2021c). Precipitation simulated by CNRM models follow the same behavior (Fig.2.B). Over-  
 267 all, the variations of the simulated global WTD follow those of precipitation, except over  
 268 the 1950 – 1970 period at a first glance. During this period, the global mean annual precipi-  
 269 tation drops because of an increase in sulfur emissions in the atmosphere (Wild, 2012). This  
 270 is not followed by a decrease of the global mean WTD, even if this decrease is simulated  
 271 over several regions such as that of south and southeast Asia (not shown). However, the  
 272 long-term evolution of the two variables are highly correlated, with a R-squared of 0.957  
 273 between the 5-yr running means of global WTD and precipitation (not shown).

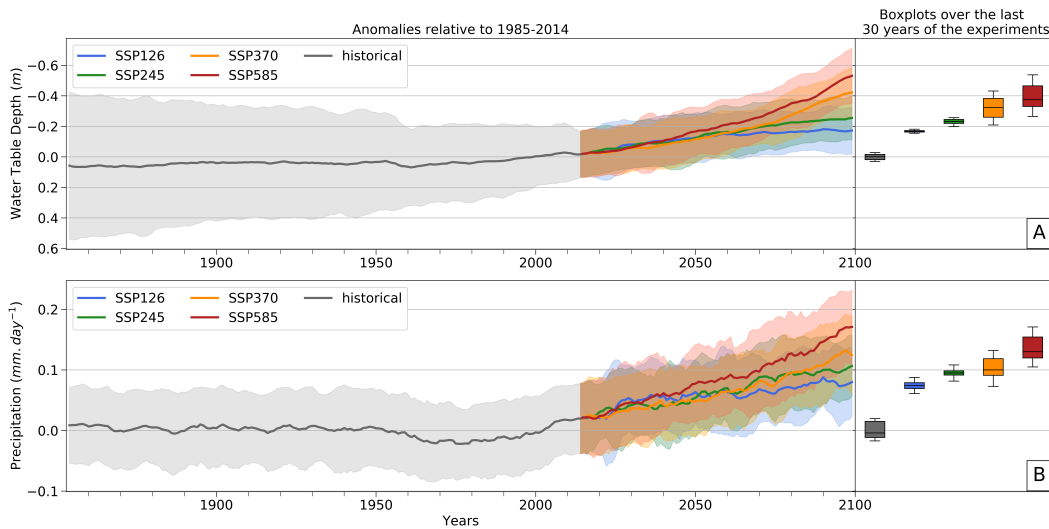


**Figure 2.** Time series (1850–2100) of the 5-year running average of global mean WTD anomalies (panel **A**) and precipitation over land anomalies (panel **B**), relative to their global average in present-day climate (1985 – 2014 period of the historical experiment), according to all scenarios. The shading areas around the global means represent the inter-member spread ( $\pm 1.64$  inter-member variance) of each experiment. Boxplots further reflect the inter-member distribution of the last 30 years of the historical experiment (1985 – 2014) and of each scenario (2071 – 2100). On the boxplots, the vertical line indicates the median, the boxplot limits the 1<sup>st</sup> and 3<sup>rd</sup> quartiles and the whiskers' length is 1.5 times the interquartile range.

274 Naturally, this global rising of groundwater due to climate change does not prevent the  
 275 occurrence of a depletion in numerous regions. The map on Fig.3.A represents the relative  
 276 difference of WTD between present-day climate (1985 – 2014) and the end of the 21<sup>st</sup>  
 277 century (2071 – 2100), following the SSP370 scenario. For readability reasons, we chose to highlight  
 278 a single scenario (see Supporting Information Fig.S4 for the other scenarios). We picked  
 279 the SSP370 because it is one of the scenarios, along with SSP245, which best match the  
 280 recent evolution of anthropogenic global fossil-fuel concentrations (Hausfather & Peters,  
 281 2020). Despite a global WTD rising of 3.8[3.6-4.0]%, these results show a clear North-South  
 282 dipole in Europe and America between groundwater rising in the north and depletion  
 283 in the south (north of the 45° latitude, approximately). The Mediterranean basin, Southern  
 284 Africa, Amazonia, central America, Australia and Southeast Asia should experience a strong  
 285 groundwater depletion, whilst central Africa, India, Northeast China, Indonesia and eastern  
 286 Argentina should see an increase of their groundwater resources with climate change. This

287 spatial pattern of the WTD changes are the same for all scenarios, the severity of which  
288 only impacts the amplitude of the changes and not their sign. However, as groundwater  
289 withdrawals are not represented in the CNRM models, this climate-driven analyse must be  
290 modulated in regions where groundwater abstractions will be significant in the future (de  
291 Graaf et al., 2019). This aspect is further discussed in section 3.4.

292 Overall, our projections of groundwater levels are consistent with the findings of the  
293 few previous studies based on CMIP5 scenarios which addressed the question of future  
294 groundwater resources at the global scale, using a fully coupled model (Wu et al., 2020) or  
295 global hydrological models run offline (Reinecke et al., 2021).

### 296 3.2 Climate drivers of the WTD changes

297 Almost everywhere, the sign of WTD changes is determined by the changes of precip-  
298 itation rather than evapotranspiration. Generally, the water table rises if the precipitation  
299 increases and vice versa, whereas an increase (respectively decrease) of evapotranspiration  
300 rarely leads to a depletion (rise) of the aquifer (Fig.3). To further investigate this matter,  
301 two linear regression models were computed for each grid point: the first one links the 5-yr  
302 running mean time-series of WTD with precipitation, and the second one also accounts for  
303 the evapotranspiration time-series. The comparison of the corresponding R-squared (Fig.4)  
304 shows that over most regions, the second regression model is only slightly better than the  
305 first one, given that the correlation between WTD and precipitation is already very high  
306 (R-squared over 0.8) and that evapotranspiration is also highly correlated to precipitation.  
307 In most places therefore, precipitation proves to be the main driver of the WTD long-term  
308 evolution, hence the widespread agreement of signs between the trends of WTD and pre-  
309 cipitation (blue and red areas on Fig.3.D).

310 There are however a few regions where the inclusion of evapotranspiration in the re-  
311 gression model considerably improves the rather low R-squared obtained with precipitation  
312 only (Fig.4), which means that evapotranspiration then plays a major role in the evolution  
313 of WTD. This is consistent with previous studies (Condon et al., 2020; Wu et al., 2020)  
314 which stressed the importance of evapotranspiration in the future evolution of groundwa-  
315 ter. The regions where the influence of evapotranspiration prevails correspond to the areas  
316 of disagreement between the precipitation and WTD changes (orange and green areas on  
317 Fig.3.D), which are in fact characterized by a lack of significance on the precipitation changes  
318 (Fig.3.B). In these cases, either the water table deepens with the increase of evapotranspi-  
319 ration (green areas on Fig.3.D) or it rises with the reduction of evapotranspiration (orange  
320 areas on Fig.3.D). It is easy to understand how evapotranspiration can increase in a warmer  
321 climate. But the decrease of evapotranspiration, in the absence of a significant change of  
322 precipitation, is somewhat surprising. Further analysis shows that it is explained by land  
323 use change features in SSP scenarios (Hurtt et al., 2020) imposed on the CNRM-ESM2-1  
324 model. For example, the deforestation of the Congo Basin in the SSP370 scenario favours  
325 groundwater recharge, as it reduces the withdrawal of soil moisture for deep rooted trees  
326 transpiration. Indeed, the conversion of forest to agricultural lands can cause an increase in  
327 groundwater recharge even if rainfall slightly decreases (Owuor et al., 2016).

328  
329 Our analysis of the drivers of WTD changes concerns the aquifers shallower than 100  
330 meters in the world's major groundwater basins, which altogether cover 40% of the land  
331 surface. However, it is reasonable to assume that aquifers which are not represented in  
332 the CNRM models will be driven by the same climate variables (i.e precipitation and evap-  
333 otranspiration when precipitation changes are not statically significant). Thus, it seems  
334 reasonable to assume that the evolution of the non-represented groundwater basins will  
335 mainly follow the precipitation and the evapotranspiration changes.

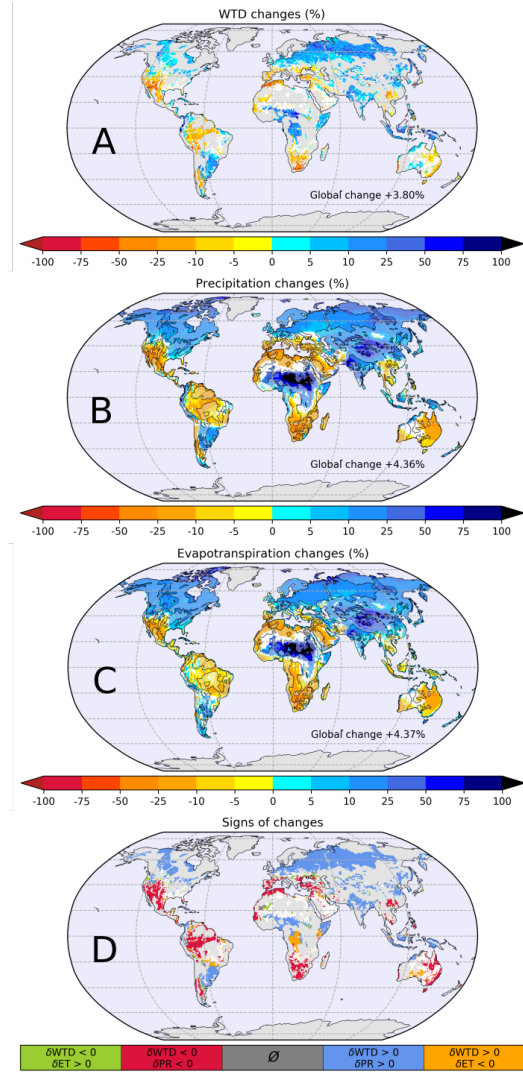


**Figure 3.** Water Table Depth (A), Precipitation (B) and Evapotranspiration (C) changes (in %) between 1985 – 2014 in the historical experiment and 2071 – 2100 in the SSP370 scenario (the values of the change averaged over land are annotated on the maps). Areas in blue (red) correspond to a future WTD rise (depletion) (A) or an increase (decrease) of precipitation/evapotranspiration (B/C). The white regions correspond to areas where the changes are not statistically significant according to the FDR test (Wilks, 2006, 2016) at a 95% level of confidence. On B and C, the localisation of the groundwater basins is emphasized to facilitate the comparison with WTD (A). D: in red and blue : comparison of the sign of WTD and precipitation (PR) changes ; in yellow and green : comparison of the sign of WTD and evapotranspiration (ET) changes wherever the sign of precipitation changes is not consistent with the sign of WTD changes. The white regions correspond to areas where WTD changes are not statistically significant.

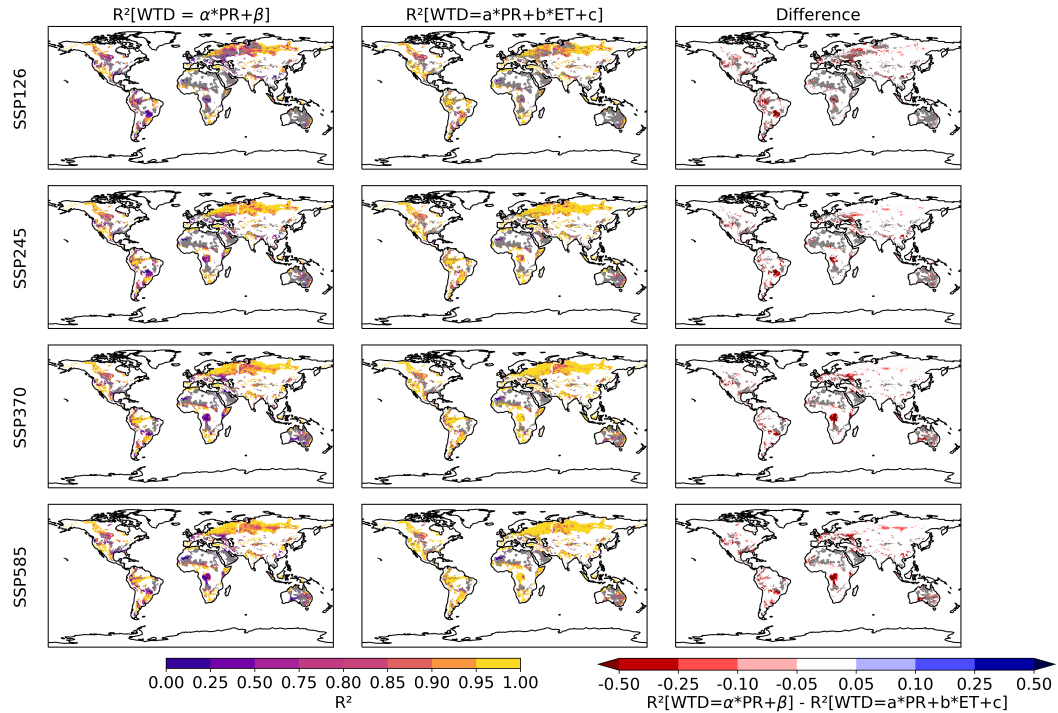


**Figure 4.** Left panel:  $R^2$  values of the linear regressions for the statistical model  $WTD = \alpha * PR + \beta$ . The linear regression is computed for each grid point with samples made of the yearly mean values of each variables for each SSP scenarios (i.e. all years from 2014 to 2100). Center panel: Same as left panel but for the statistical model  $WTD = a * PR + b * ET + c$ . Right panel:  $R^2$  values differences between the second model (center panel) and the first one (left panel). Red areas correspond to areas where WTD changes are better correlated with both precipitation and evapotranspiration changes than with precipitation changes only.

336

### 3.3 Multi-model analysis

337

338

339

340

341

342

343

344

345

To further explore the uncertainties on the groundwater response to climate change in the CMIP6 experiments, it would be necessary to conduct a multi-model analysis. Unfortunately, in the CMIP6 cohort, the CNRM models are ones of the few which compute water table depth, but the only one using an hydrogeological modelling approach. The question can not therefore be addressed directly. We can however confront the CNRM models' projections of precipitation and evapotranspiration to those simulated by 18 other state-of-the-art climate models contributing to CMIP6. Given that these two climate variables drive the long-term trends of WTD, they are responsible for a significant part of the uncertainties associated with the projections of WTD.

346

347

348

349

350

351

352

353

354

Results of this multi-model analysis show that overall, the CNRM models agree with the other CMIP6 models on the evolution of precipitation and evapotranspiration over land surfaces in the future (Fig.5, Fig.6, and Supporting Information Fig.S7 and S8). The CNRM models global time-series (1850-2100) fall within the range of the inter-model spread. The spatial patterns of precipitation and evapotranspiration future changes of the CNRM models are also in agreement with the CMIP6 multi-model ensemble results (Fig.7). This naturally reflects the findings already reported in the AR6 (IPCC, 2021a), as well as in the previous IPCC assessment report (IPCC, 2013b). In both cases (CNRM models and CMIP6 ensemble), the future climate is projected to be wetter and more humid in most regions

355 outside of the Mediterranean, Australia, southern Africa, Brazil and Central America. The  
 356 few areas where the CNRM models results disagree with the CMIP6 multi-model mean on  
 357 the sign of the changes correspond to transition zones between regions of humidification  
 358 and drying. And in most of these places, the climate change signal is not statistically  
 359 significant in the CNRM models. This agreement between the CNRM models and the  
 360 CMIP6 multi-model ensembles regarding the climatic drivers of WTD changes provides an  
 361 increased confidence in our projections of groundwater levels.

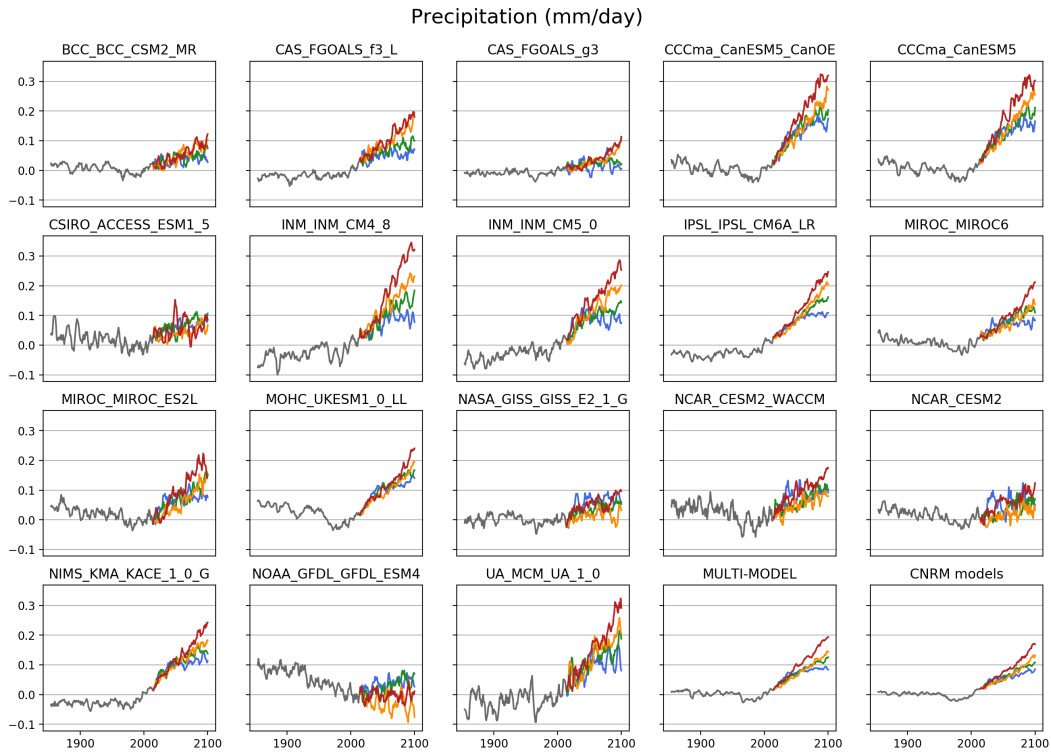


**Figure 5.** Times-series (1850 – 2100) of the 5-yr running means of global land precipitation anomalies (relatively to 1985 – 2014) for each SSP scenario: ensemble means of the model references in Table.1 to the exclusion of the CNRM models, multi-model ensemble of these ensemble means, and ensemble mean of the CNRM models. The slope of the linear regression of each time-series is given in Supporting Information Fig.7

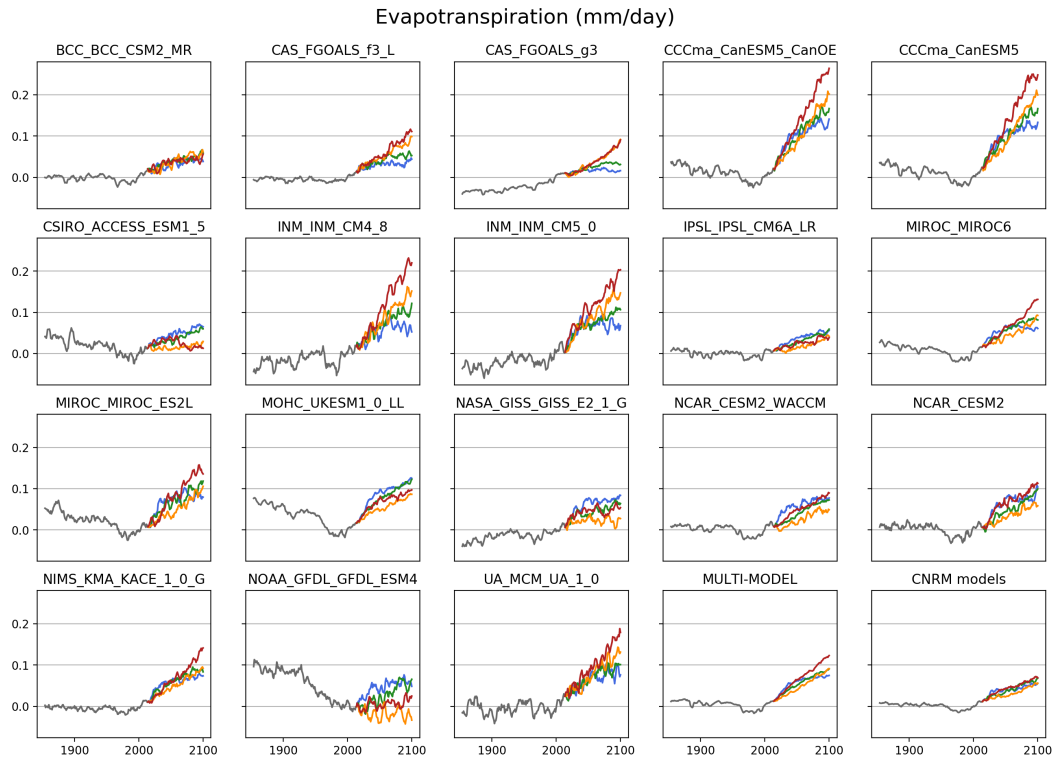


**Figure 6.** Same as Fig.5 but for evapotranspiration. The slope of the linear regression of each time-series is given in Supporting Information Fig.8

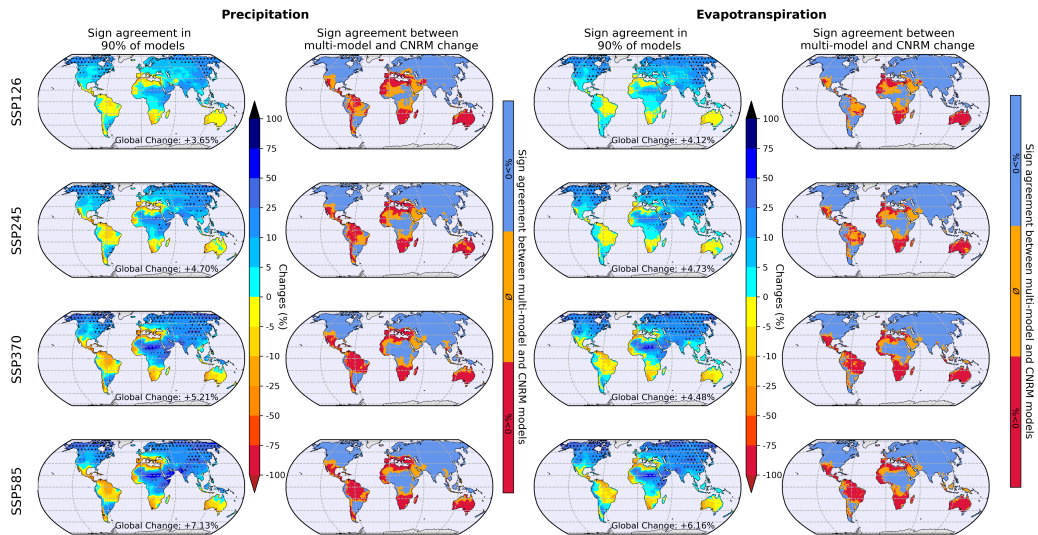


**Figure 7.** First column: Multi-model ensemble (excluding the CNRM models) of precipitation relative change (in %) between 1985 – 2014 and 2071 – 2100 for each SSP scenario. Black dots indicate areas where 90% of the models agree on the sign of the change. Second column: Comparison of the precipitation multi-model change with the change simulated by the CNRM models. In blue: common increase ; in red: common decrease ; in orange: opposite signs of change. Third and fourth columns: same as the first and second columns but for evapotranspiration.

362

### 3.4 Potential humans impacts in 2100

363

364

365

366

Our projections of future groundwater levels can also be analysed in terms of the foreseeable impact on human water risks. The goal is to determine how the population might be impacted by the climate-driven variations of WTD, and how the lack of human withdrawals representation in our modeling framework is likely to modulate these impacts.

367

368

369

370

371

As already said, because human withdrawals of groundwater are not represented in the CNRM models, our projections of WTD might be biased in regions where the inclusion of groundwater pumping would lead to shallower water tables. Indeed, it has been shown that groundwater pumping can cause or worsen the depletion of aquifer basins (IPCC, 2021a, 2022b; Famiglietti, 2014; Doll et al., 2009; Gurdak, 2017; Wu et al., 2020).

372

373

374

375

376

377

378

379

380

381

382

383

384

Irrigation accounts for 70% of groundwater withdrawals (Siebert et al., 2010) and thus constitutes the main use of groundwater. Using maps of areas currently equipped for irrigation (see Supporting Information Fig.S3), we find that 2.8% of the areas located over the large groundwater basins are equipped for irrigation and 0.9% specifically for groundwater irrigation. But even if these global means of areas equipped for irrigation are low, in the regions where they are not negligible, our climate-driven projections of WTD changes are likely to be modulated by groundwater pumping for irrigation. By 2100, most of the future scenarios of global irrigated areas show either a stagnation of irrigated areas or a slight increase followed by a decrease. In the few scenarios projecting an increase of the global irrigated area, its future extent does not exceed twice the present-day values computed over the historical period (Hurtt et al., 2020). Given these projections and the uncertainties on the possible change in the geographical distribution of irrigated regions, we find reasonable to base our analysis on the currently irrigated areas, as done in de Graaf et al. (2019).

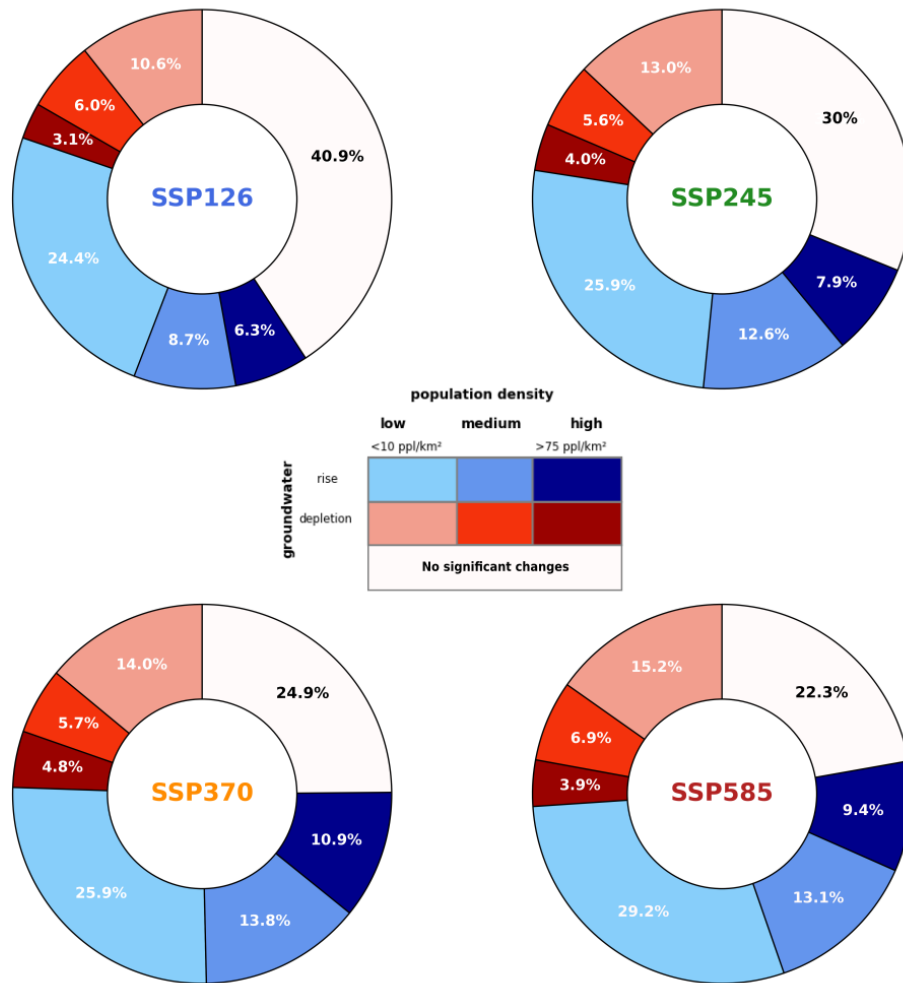


**Figure 8.** Share of area covered by the world's major groundwater basins where groundwater levels are projected to rise (blue) and to deplete (red). The color intensity indicates the projected population density (people per km<sup>2</sup>) in 2100. The light colours correspond to areas with fewer than 10 inhabitants per square kilometer and the dark colours to areas with more than 75 inhabitants per square kilometer. The white regions correspond to areas where WTD changes between 1985 – 2014 and 2071 – 2100 are not statistically significant.

385 Four regions of substantial groundwater irrigation stand out: the northern China Plain,  
 386 North India (the north Indus and Ganges valleys), the US Great Plains and the Central  
 387 Valley in California. In these regions, satellite measurements and groundwater wells data  
 388 show that groundwater is already depleting (Rodell et al., 2009; Panda et al., 2021; Scanlon  
 389 et al., 2012; Doll et al., 2012; Jasechko & Perrone, 2021). Furthermore, using a hydrological  
 390 model which estimates groundwater withdrawals, de Graaf et al. (2019) highlights these  
 391 regions as the four notable depletion hot spots at the end of the 21<sup>st</sup> century (see Extended  
 392 Data Fig.2 in de Graaf et al. (2019)). In these regions, the lack of groundwater withdrawals  
 393 is thus likely to affect our projection of WTD changes.

394 We further discuss this point using the future population density. Indeed, the compar-  
 395 ison of areas currently equipped for irrigation with the world's population density (see

Fig.S3 and Fig.S1 in Supporting Information) shows that except in the US Great Plains, irrigated areas are densely populated, while the reverse is not necessarily true. In addition, it has been shown in other studies that population growth and socio-economic development combined with climate change, are the major contributors to the water use increase (Shen et al., 2014). Future population density therefore allows to determine where groundwater irrigation could actually matter and also integrates other uses of groundwater (domestic and industrial uses). Essentially, this leads us to consider that in addition to the four previously mentioned regions (the northern China Plain, North India, the US Great Plains and Central Valley), our climate-driven projections of WTD changes are also likely to be modulated by human withdrawals in a few other densely populated areas located in Northern Europe and Central Africa. However, outside of these regions, our analysis suggests that our climate driven-estimates should not be biased by the lack of groundwater irrigation.

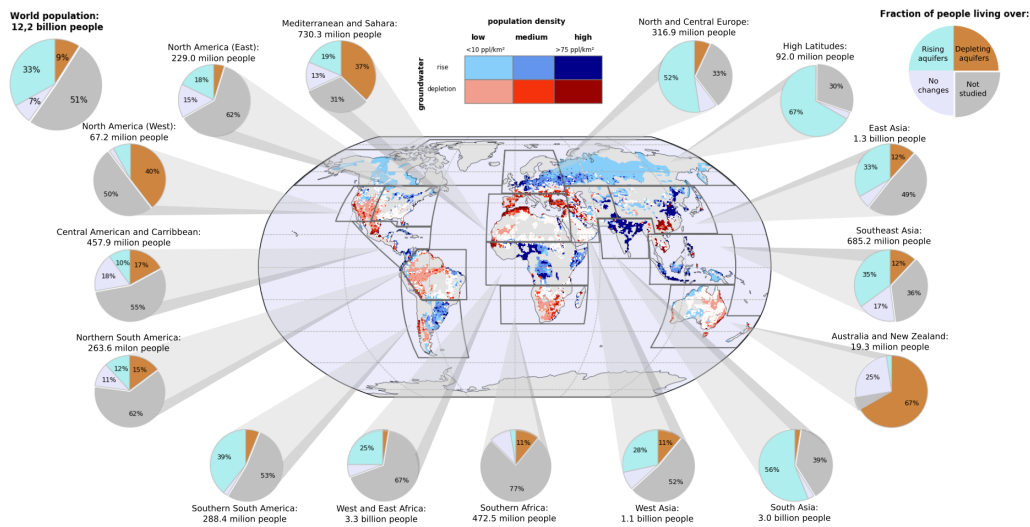


**Figure 9.** Evolution of WTD and population density in 2100 with the SSP370 scenario. As in Fig.8, aquifer areas are coloured blue (red) if groundwater levels are projected to rise (deepen), whilst the color intensity indicates the projected population density in 2100. The global pie chart (left hand corner) represents the distribution of the world's population which could be affected by a rising (turquoise) or a depletion (brown) of groundwater levels, or which is likely to live above an aquifer basin where future changes are not significant (white) or over unstudied areas (grey). The same pie charts are given for each selected region, defined as those used in the Atlas of Global and Regional Climate Projections in the Annex 1 of the IPCC AR5 (IPCC, 2013a).

Figures 8 and 9 gather the information on WTD and population density in 2100. Three different types of situations can be identified with these figures.

The first one corresponds to sparsely and moderately populated areas where aquifers are projected to rise with climate-driven changes, such as the high latitudes or parts of Northern Europe (light and medium blue areas in Fig.9). In these regions, water stress should not be an issue in the future, as the risk of human withdrawal exceeding the projected increase of groundwater storage can be considered as moderate and depletion estimates at the end of the century by de Graaf et al (2019) are weak or negligible. The projected increase of precipitation with climate change could lead to a replenishment of currently depleting aquifers or a further increase of groundwater resources in these regions (albeit less than projected in our simulations). As the groundwater is the primary source of streamflow during dry periods, the increase of groundwater levels could benefit to rivers, lakes and

wetlands by supplying baseflow and maintaining ecosystems (Winter et al., 1998; Fan et al., 2013), although the rising of the annual mean of WTD does not necessarily translate into a rising during the driest months. There could however be an increased flood risk. Indeed, the saturation of aquifers and overlaying soils can foster or worsen spring freshets and floods associated with periods of intense or prolonged precipitation, as it was the case in 2000 – 2001 in England or in 2013 in Alberta (Abboud et al., 2018; Adams et al., 2010).

The second case corresponds to highly populated areas such as South Asia or central Africa, where groundwater levels are also projected to rise (dark blue areas in Fig.9). With a high population density however, human water requirements are expected to be significant and even increase with climate change and/or the growth of the population. The projected increase of groundwater storage should therefore be reversed and become a decrease, as is already the case in the Ganges valley in North India and in North China where groundwater is already depleting because of withdrawals (Rodell et al., 2009; Siebert et al., 2010; Panda et al., 2021). Furthermore, de Graaf et al. (2019) identified these two latter regions as being amongst the four where groundwater should deplete the most by the end of the century. Here, the projected increase of precipitation with climate change could be entirely compensated, and even surpassed, by a growing human strain on groundwater.

The third situation corresponds to regions where the mean regional WTD is projected to deepen, corresponding to a depletion of groundwater, even without taking into account human withdrawal (red regions in Fig.9), such as the Mediterranean, southern Africa and southwestern USA. This could be a huge problem in populated areas where the drop of WTD will widen the risk of water stress, especially in regions that are already groundwater-dependant (Iglesias et al., 2007) such as the Central Valley in California in the US Great Plains (de Graaf et al., 2019). Again, in these regions, the real future depletion should be much stronger than projected, as human withdrawals are not taken into account in the CNRM models and are likely to increase in the future.

If we consider the area covered by the world's major groundwater basins we studied here, we find that depending on the scenario, 33[28-39]% (in SSP126) to 42[41-45]% (in SSP585) of this surface is affected by a climate-driven rise of groundwater levels which is not likely to be turned into a depletion with groundwater withdrawal (light and medium blue areas on Fig.8). 0.1[0.1-0.2] (in SSP126) to 0.3[0.3-0.4] (in SSP370) billions people are projected to live in these regions, which corresponds to 1.7[1.5-2.2]% to 2.2[2.2-2.4]% of the future world's population. For 6.3[5.9-8.0]% (in SSP126) to 10.9[10.5-11.1]% (in SSP370) of the world's major groundwater basins surface, the climate-driven rise of water tables should be reversed into a depletion, as these highly populated regions correspond to regions of intense groundwater withdrawals (dark blue regions in Fig.9). 1.3[1.2-1.5] (in SSP126) to 3.8[3.7-3.9] (in SSP370) billions people are projected to live in these regions, which corresponds to 19[18-22]% to 31[31-30]% of the future world's population. And 20[19-24]% (in SSP126) to 26[25-29]% (in SSP370) of the world's major groundwater basins surface are projected to experience a climate-driven groundwater depletion, which can only be worsened with human withdrawals (red areas on Fig.9). 0.6[0.6-0.8] (in SSP126) to 1.1[1.0-1.1] (in SSP370) billions people are projected to live in these regions, which corresponds to 10[9-11]% and to 9[8-9]% of the future world's population. The global pie chart on Fig.9 indicates that, for the SSP370 scenario, 49% of the world's population in 2100 is projected to live in regions located above large groundwater basins and is therefore likely to rely on groundwater resources (see Supporting Information Fig.S6 for the other scenarios).

But people living outside these large groundwater basins could however still partly rely on groundwater resources, either because they live near a large aquifer or because they exploit more localised aquifers. Considering all land surfaces (i.e. whether or not they are located above large groundwater basins) in each of the regions defined on Figure 9, we find that for the SSP370 scenario, in 2100, 17% of the world's population (2.1 billion people) live

472 in regions where climate change mostly induces a rise of groundwater which is not likely to  
473 be compensated by withdrawals. 68% of the world's population (8.3 billion people) live in  
474 regions where although groundwater levels are mostly projected to rise with climate change,  
475 human withdrawals should reverse this signal into a groundwater depletion. And 15% of  
476 the world's population (1.8 billion people) live in regions where water tables are mostly  
477 projected to deepen even without taking into account withdrawals. Note that the computa-  
478 tion of confidence intervals does not apply here, as we consider the dominant sign of WTD  
479 changes over large regions and it remains the same throughout the bootstrap resampling of  
480 our ensemble of simulations.  
481

## 482 4 Summary and prospect

483 The CNRM models provide a spatially contrasted response of groundwater to climate  
484 change throughout the 21<sup>st</sup> century, over the 218 world's major groundwater basins. Over  
485 Europe and North America, we find a rising of groundwater in the North and a deple-  
486 tion in the South. Elsewhere, climate-driven evolution of WTD lead mostly to a rising of  
487 groundwater in central Africa, Northeast China, India, Indonesia and southern America,  
488 whilst the Mediterranean region, Southern Africa, Amazonia, central America, Australia  
489 and Southeast Asia are projected to experience a strong groundwater depletion.

490 Our analysis shows that precipitation is the main driver of these climate-driven changes  
491 of groundwater levels and that the contribution of evapotranspiration dominates only in  
492 regions where precipitation is not projected to significantly change in the future. The con-  
493 fidence in our estimates of the long-term climate-driven evolution of groundwater level is  
494 increased by the agreement between our projections of its two main climatic drivers (pre-  
495 cipitation and evapotranspiration) and CMIP6 multi-model ensemble projections of these  
496 variables. However, in some regions, this response of groundwater resources to climate  
497 change should be balanced by human groundwater withdrawals which are not accounted for  
498 our climate models.

499 Our discussion on this point is firstly based on the analysis of FAO maps of present-day  
500 irrigated areas and projections of future population densities. We complement it with the  
501 comparison of our results on climate-driven WTD changes with those of the recent study  
502 of de Graaf et al. (2019). It points out the fact that the highly populated regions where  
503 a climate-driven rising is projected should in fact see their groundwater resources decrease  
504 due to human withdrawals. Among these regions, we find the North China Plain, the  
505 Ganges and northern Indus valleys where groundwater is already depleting and which de  
506 Graaf et al. (2019) identified as hot spots of future depletion. And while these regions only  
507 represent 6.3[5.9-8.0]% to 10.9[10.5-11.1]% of the surface covered by the 218 world's major  
508 aquifer basins and 2.7[2.5-3.4]% to 4.7[4.5-4.8]% of the total land surface (depending on the  
509 scenario), they amount for a large part of the future world's population. Indeed, 19[18-22]%  
510 to 31[31-30]% of the future world's population live in these regions and thus should face  
511 water scarcity issues, as the projected increase of precipitation are unlikely to compensate  
512 the depletion of groundwater caused by human withdrawals (unless those are reduced in  
513 the future). An additional  $\sim 10\%$  of the future world's population should also face water  
514 scarcity issues, as they are projected to live in regions where the climate-driven changes  
515 of WTD induce a depletion of groundwater, which should be worsened by withdrawal in  
516 densely populated areas. On the contrary, only  $\sim 2\%$  of the future world's population is  
517 projected to live in regions where the climate-driven increase of groundwater resource is  
518 unlikely to be offset by human withdrawals, although these regions represent 33[28-39]% to  
519 42[41-45]% of the surface covered by major's aquifer basins (14[12-17]% to 18[18-19]% of the  
520 total land surface). In these latter regions, the increase of groundwater levels could benefit  
521 to rivers, lakes and wetlands by supplying baseflow and maintaining ecosystems. However,  
522 the flood risks could be increased.

523 To further assess the uncertainties on the groundwater response to future climate  
 524 change, we argue in favor of a more comprehensive multi-model approach, which would  
 525 rely on coupled global climate models or Earth system models including a realistic rep-  
 526 resentation of groundwater processes. Other members of the climate and/or hydrology  
 527 modelling communities have also advocated for the development and use of such holistic  
 528 global models (Fan et al., 2013; Clark et al., 2015; Boe, 2021; Gleeson et al., 2021). Improv-  
 529 ing and increasing our confidence in the projections of future groundwater resources does  
 530 indeed constitute a high-stake issue because it conditions the implementation of suitable  
 531 mitigation and adaptation plans to counter the widening risks of water scarcity (Famiglietti,  
 532 2014; Thomas & Famiglietti, 2019).

533 Beyond the necessity to account for a valuable representation of groundwater processes  
 534 in global climate models, we emphasize the need to consider the representation of ground-  
 535 water pumping and irrigation processes (groundwater contributes to 42% of irrigated water  
 536 (Doll et al., 2012), which amounts to 70% of human groundwater intake (Siebert et al.,  
 537 2010)). As we discussed in section 3.4, the consideration of human groundwater withdrawal  
 538 and its future evolution is likely to locally modulate, and in some places even invert, the  
 539 impact of the future climate change on groundwater (Wada, 2016; Wu et al., 2020; de Graaf  
 540 et al., 2019). This modulation of the groundwater evolution, along with the modification  
 541 of evapotranspiration and/or hydrological processes induced by irrigation, could affect in  
 542 return the projected climate, hence the need to include these processes in fully coupled  
 543 climate models.

## 544 5 Open Research

545 All the CNRM climate models and multi-model ensemble data are freely available  
 546 on the ESGF website (<https://esgf-node.ipsl.upmc.fr/search/cmip6-ips1/>). The  
 547 SEDAC data are available at [https://sedac.ciesin.columbia.edu/data/set/gpw-v4-](https://sedac.ciesin.columbia.edu/data/set/gpw-v4-population-density-rev11)  
 548 [population-density-rev11](https://sedac.ciesin.columbia.edu/data/set/gpw-v4-population-density-rev11), the CMIP6 projection of population density by country at  
 549 <https://tntcat.iiasa.ac.at/SspDb/dsd?Action=htmlpage&page=welcome>, the GMTED  
 550 1km topography data at [https://topotools.cr.usgs.gov/gmted\\_viewer/](https://topotools.cr.usgs.gov/gmted_viewer/), the global map  
 551 of the groundwater resources of the world from WHYMAP at <http://www.whymap.org>, and  
 552 the the principal aquifers of the conterminous United States from the USGS at [https://](https://water.usgs.gov/GIS/metadata/usgswrd/XML/aquifers_us.xml)  
 553 [water.usgs.gov/GIS/metadata/usgswrd/XML/aquifers\\_us.xml](https://water.usgs.gov/GIS/metadata/usgswrd/XML/aquifers_us.xml). The irrigation datas from  
 554 FAO are available at <https://data.apps.fao.org/aquamaps/>.

## 555 Acknowledgments

556 The authors would like to thank Christine Delire, Herve Douville, Julien Boe and Florence  
 557 Habets for their useful comments. The authors are also grateful to the anonymous reviewers.  
 558 This work is supported by the “Centre National de Recherches Météorologiques” (CNRM)  
 559 of Météo-France and the “Centre National de la Recherche Scientifique” (CNRS) of the  
 560 French research ministry. This paper has received support from the European Union’s  
 561 Horizon 2020 research and innovation programme under Grant Agreement N° 101003536  
 562 (ESM2025 – Earth System Models for the Future).

## 563 References

- 564 Abboud, J. M., Ryan, M. C., & Osborn, G. D. (2018, dec). Groundwater flooding in  
 565 a river-connected alluvial aquifer. *Journal of Flood Risk Management*, 11(4). doi:  
 566 10.1111/JFR3.12334  
 567 Adams, B., Bloomfield, J. P., Gallagher, A. J., Jackson, C. R., Rutter, H. K., & Williams,  
 568 A. T. (2010). An early warning system for groundwater flooding in the Chalk.  
 569 *Quarterly Journal of Engineering Geology and Hydrogeology*, 43(2), 185–193. doi:  
 570 10.1144/1470-9236/09-026

- 571 Alley, W. M., Healy, R. W., LaBaugh, J. W., & Reilly, T. E. (2002). Flow and storage in  
572 groundwater systems. *Science*, *296*(5575), 1985–1990. doi: 10.1126/science.1067123
- 573 Amanambu, A. C., Obarein, O. A., Mossa, J., Li, L., Ayeni, S. S., Balogun, O., ... Ochege,  
574 F. U. (2020). Groundwater system and climate change: Present status and future  
575 considerations. *Journal of Hydrology*, *589*(May), 125163. Retrieved from [https://](https://doi.org/10.1016/j.jhydrol.2020.125163)  
576 [doi.org/10.1016/j.jhydrol.2020.125163](https://doi.org/10.1016/j.jhydrol.2020.125163) doi: 10.1016/j.jhydrol.2020.125163
- 577 Anyah, R. O., Weaver, C. P., Miguez-Macho, G., Fan, Y., & Robock, A. (2008). Incorporat-  
578 ing water table dynamics in climate modeling: 3. Simulated groundwater influence on  
579 coupled land-atmosphere variability. *Journal of Geophysical Research Atmospheres*,  
580 *113*(7). doi: 10.1029/2007JD009087
- 581 Boe, J. (2021). The physiological effect of CO<sub>2</sub> on the hydrological cycle in summer over  
582 Europe and land-atmosphere interactions. *Climatic Change*, *167*(1-2), 1–20. doi:  
583 10.1007/s10584-021-03173-2
- 584 Cazenave, A., Dieng, H.-b., Meyssignac, B., Schuckmann, K. V., Decharme, B., & Berthier,  
585 E. (2014). The rate of sea-level rise. *Nature Climate Change*, *4*(May), 358–361. doi:  
586 10.1038/NCLIMATE2159
- 587 Clark, M. P., Fan, Y., Lawrence, D. M., Adam, J. C., Bolster, D., Gochis, D. J., ...  
588 Maxwell, R. M. (2015). Improving the representation of hydrologic processes in  
589 Earth SystemModels. *Water Resources Research*, *51*, 5929–5956. doi: 10.1002/  
590 2015WR017096.Received
- 591 Condon, L. E., Atchley, A. L., & Maxwell, R. M. (2020). Evapotranspiration depletes  
592 groundwater under warming over the contiguous United States. *Nature Communi-*  
593 *cations*, *11*(1). Retrieved from <http://dx.doi.org/10.1038/s41467-020-14688-0>  
594 doi: 10.1038/s41467-020-14688-0
- 595 Decharme, B., Delire, C., Minvielle, M., Colin, J., Vergnes, J. P., Alias, A., ... Voldoire,  
596 A. (2019). Recent Changes in the ISBA-CTrip Land Surface System for Use in  
597 the CNRM-CM6 Climate Model and in Global Off-Line Hydrological Applications.  
598 *Journal of Advances in Modeling Earth Systems*, *11*(5), 1207–1252. doi: 10.1029/  
599 2018MS001545
- 600 de Graaf, I. E., Gleeson, T., (Rens) van Beek, L. P., Sutanudjaja, E. H., & Bierkens,  
601 M. F. (2019). Environmental flow limits to global groundwater pumping. *Nature*,  
602 *574*(7776), 90–94. Retrieved from <http://dx.doi.org/10.1038/s41586-019-1594-4>  
603 doi: 10.1038/s41586-019-1594-4
- 604 Delire, C., Seferian, R., Decharme, B., Alkama, R., Calvet, J. C., Carrer, D., ... Tzanos, D.  
605 (2020). The Global Land Carbon Cycle Simulated With ISBA-CTrip: Improvements  
606 Over the Last Decade. *Journal of Advances in Modeling Earth Systems*, *12*(9), 1–31.  
607 doi: 10.1029/2019MS001886
- 608 Doll, P., Fiedler, K., & Zhang, J. (2009). Global-scale analysis of river flow alterations due  
609 to water withdrawals and reservoirs. *Hydrology and Earth System Sciences*, *13*(12),  
610 2413–2432. doi: 10.5194/hess-13-2413-2009
- 611 Doll, P., Hoffmann-Dobrev, H., Portmann, F. T., Siebert, S., Eicker, A., Rodell, M., ...  
612 Scanlon, B. R. (2012). Impact of water withdrawals from groundwater and surface  
613 water on continental water storage variations. *Journal of Geodynamics*, *59-60*, 143–  
614 156. Retrieved from <http://dx.doi.org/10.1016/j.jog.2011.05.001> doi: 10  
615 .1016/j.jog.2011.05.001
- 616 Douville, H., Ribes, A., Decharme, B., Alkama, R., & Sheffield, J. (2013). Anthropogenic  
617 influence on multidecadal changes in reconstructed global evapotranspiration. *Nat-*  
618 *ure Climate Change*, *3*(1), 59–62. Retrieved from [http://dx.doi.org/10.1038/](http://dx.doi.org/10.1038/nclimate1632)  
619 [nclimate1632](http://dx.doi.org/10.1038/nclimate1632) doi: 10.1038/nclimate1632
- 620 Durr, H. H., Meybeck, M., & Durr, S. H. (2005). Lithologic composition of the Earth's  
621 continental surfaces derived from a new digital map emphasizing riverine material  
622 transfer. *Global Biogeochemical Cycles*, *19*(4), 1–23. doi: 10.1029/2005GB002515
- 623 Eyring, V., Bony, S., Meehl, G. A., Senior, C. A., Stevens, B., Stouffer, R. J., & Taylor,  
624 K. E. (2016). Overview of the Coupled Model Intercomparison Project Phase 6  
625 (CMIP6) experimental design and organization. *Geoscientific Model Development*,

- 626 9(5), 1937–1958. doi: 10.5194/gmd-9-1937-2016
- 627 Famiglietti, J. S. (2014). The global groundwater crisis. *Nature Climate Change*, 4(11),  
628 945–948. Retrieved from <http://dx.doi.org/10.1038/nclimate2425> doi: 10.1038/  
629 nclimate2425
- 630 Fan, Y., Clark, M., Lawrence, D. M., Swenson, S., Band, L. E., & Brantley, S. L.  
631 (2019). Hillslope Hydrology in Global Change Research and Earth System Mod-  
632 eling Water Resources Research. *Water Resources Research*, 55, 1737–1772. doi:  
633 10.1029/2018WR023903
- 634 Fan, Y., Li, H., & Miguez-Macho, G. (2013). Global patterns of Groundwater Table Depth.  
635 *Science*, 339(6122), 940–943. doi: 10.1126/science.1229881
- 636 Gleeson, T., Wagener, T., Doll, P., Zipper, S. C., West, C., Wada, Y., ... Maxwell, R.  
637 (2021). GMD perspective: The quest to improve the evaluation of groundwater rep-  
638 resentation in continental- to global-scale models. *Geoscientific Model Development*,  
639 14(April), 7545–7571.
- 640 Green, T. R., Taniguchi, M., Kooi, H., Gurdak, J. J., Allen, D. M., Hiscock, K. M., ...  
641 Aureli, A. (2011). Beneath the surface of global change: Impacts of climate change on  
642 groundwater. *Journal of Hydrology*, 405(3-4), 532–560. doi: 10.1016/j.jhydrol.2011  
643 .05.002
- 644 Gurdak, J. J. (2017). Climate-induced pumping. *Nature Geoscience*, 10.
- 645 Hausfather, Z., & Peters, G. P. (2020). Emissions – the ‘business as usual’ story is misleading.  
646 *Nature*, 577(7792), 618–620. doi: 10.1038/d41586-020-00177-3
- 647 Hurtt, G. C., Chini, L., Sahajpal, R., Frohling, S., Bodirsky, B. L., Calvin, K., ... Hasegawa,  
648 T. (2020). Harmonization of global land use change and management for the period  
649 850 – 2100 ( LUH2 ) for CMIP6. *Geoscientific Model Development*, 13, 5425–5464.
- 650 Iglesias, A., Garrote, L., Flores, F., & Moneo, M. (2007). Challenges to manage the  
651 risk of water scarcity and climate change in the Mediterranean. *Water Resources*  
652 *Management*, 21(5), 775–788. doi: 10.1007/s11269-006-9111-6
- 653 IPCC. (2013a). Annex I: Atlas of Global and Regional Climate Projections [van Olden-  
654 borgh, G.J., M. Collins, J. Arblaster, J.H. Christensen, J. Marotzke, S.B. Power, M.  
655 Rummukainen and T. Zhou (eds.)]. In: *Climate Change 2013: The Physical Science*  
656 *Basis. Contribution of Working Group I to the Fifth Assessment Report of the In-*  
657 *tergovernmental Panel on Climate Change* [Stocker, T.F., D. Qin, G.-K. Plattner, M.  
658 Tignor, S.K. Allen, J. Boschung, A. Nauels, Y. Xia, V. Bex and P.M. Midgley (eds.)].  
659 Cambridge University Press, Cambridge, United Kingdom and New York, NY, U.
- 660 IPCC. (2013b). *Climate Change 2013: The Physical Science Basis. Contribution of Working*  
661 *Group I to the Fifth Assessment Report of the Intergovernmental Panel on Climate*  
662 *Change* [Stocker, T.F., D. Qin, G.-K. Plattner, M. Tignor, S.K. Allen, J. Boschung,  
663 A. Nauels, Y. Xia, V. Bex and P.M. Midgley (eds.)]. Cambridge University Press,  
664 Cambridge, United Kingdom and New York, NY, USA, 1535 pp.
- 665 IPCC. (2021a). *Climate Change 2021: The Physical Science Basis. Contribution of Working*  
666 *Group I to the Sixth Assessment Report of the Intergovernmental Panel on Climate*  
667 *Change*[Masson-Delmotte, V., P. Zhai, A. Pirani, S.L. Connors, C. Péan, S. Berger,  
668 N. Caud, Y. Chen, L. Goldfarb, M.I. Gomis, M. Huang, K. Leitzell, E. Lonnoy, J.B.R.  
669 Matthews, T.K. Maycock, T. Waterfield, O. Yelekçi, R. Yu, and B. Zhou (eds.)]. Cam-  
670 bridge University Press. In Press.
- 671 IPCC. (2021b). Douville, H., K. Raghavan, J. Renwick, R.P. Allan, P.A. Arias, M. Barlow,  
672 R. Cerezo-Mota, A. Cherchi, T.Y. Gan, J. Gergis, D. Jiang, A. Khan, W. Pokam  
673 Mba, D. Rosenfeld, J. Tierney, and O. Zolina, 2021: Water Cycle Changes. In *Climate*  
674 *Change 2021: The Physical Science Basis. Contribution of Working Group I to the*  
675 *Sixth Assessment Report of the Intergovernmental Panel on Climate Change*[Masson-  
676 Delmotte, V., P. Zhai, A. Pirani, S.L. Connors, C. Péan, S. Berger, N. Caud, Y. Chen,  
677 L. Goldfarb, M.I. Gomis, M. Huang, K. Leitzell, E. Lonnoy, J.B.R. Matthews, T.K.  
678 Maycock, T. Waterfield, O. Yelekçi, R. Yu, and B. Zhou (eds.)]. Cambridge University  
679 Press. In Press.
- 680 IPCC. (2021c). Lee, J.-Y., J. Marotzke, G. Bala, L. Cao, S. Corti, J.P. Dunne, F. En-

- 681 gelbrecht, E. Fischer, J.C. Fyfe, C. Jones, A. Maycock, J. Mutemi, O. Ndiaye, S.  
 682 Panickal, and T. Zhou:2021, Future Global Climate: Scenario-Based Projections and  
 683 Near-Term Information. In *Climate Change 2021: The Physical Science Basis. Contri-*  
 684 *bution of Working Group I to the Sixth Assessment Report of the Intergovernmental*  
 685 *Panel on Climate Change* [Masson-Delmotte, V., P. Zhai, A. Pirani, S.L. Connors, C.  
 686 Péan, S. Berger, N. Caud, Y. Chen, L. Goldfarb, M.I. Gomis, M. Huang, K. Leitzell,  
 687 E. Lonnoy, J.B.R. Matthews, T.K. Maycock, T. Waterfield, O. Yelekçi, R. Yu, and B.  
 688 Zhou (eds.)]. Cambridge University Press. In Press.
- 689 IPCC. (2022a). Caretta, M.A., A. Mukherji, M. Arfanuzzaman, R.A. Betts, A. Gelfan,  
 690 Y. Hirabayashi, T.K. Lissner, J. Liu, E. Lopez Gunn, R. Morgan, S. Mwanga, and  
 691 S. Supratid, 2022: Water. In: *Climate Change 2022: Impacts, Adaptation, and Vul-*  
 692 *nerability. Contribution of Working Group II to the Sixth Assessment Report of the*  
 693 *Intergovernmental Panel on Climate Change* [H.-O. Pörtner, D.C. Roberts, M. Tignor,  
 694 E.S. Poloczanska, K. Mintenbeck, A. Alegría, M. Craig, S. Langsdorf, S. Lösschke, V.  
 695 Möller, A. Okem, B. Rama (eds.)]. Cambridge University Press. In Press.
- 696 IPCC. (2022b). IPCC, 2022: *Climate Change 2022: Impacts, Adaptation, and Vulner-*  
 697 *ability. Contribution of Working Group II to the Sixth Assessment Report of the*  
 698 *Intergovernmental Panel on Climate Change* [H.-O. Pörtner, D.C. Roberts, M. Tig-  
 699 nor, E.S. Poloczanska, K. Mintenbeck, A. Alegría, M. Craig, S. Langsdorf, S. Lösschke,  
 700 V. Möller, A. Okem, B. Rama (eds.)]. Cambridge University Press. In Press.
- 701 Jasechko, S., & Perrone, D. (2021). Global groundwater wells at risk of running dry. *Science*,  
 702 *372*(6540), 418–421. doi: 10.1126/science.abc2755
- 703 Kay, J. E., Deser, C., Phillips, A., Mai, A., Hannay, A., Strand, G., . . . Versteinstein, M.  
 704 (2015). The Community Earth System Model (CESM) Large Ensemble Project: a  
 705 community resource for studying climate change in the presence of internal climate  
 706 variability. *Bulletin of the American Meteorological Society*, *96*(August), 1333–1350.  
 707 doi: 10.1175/BAMS-D-13-00255.1
- 708 KC, S., & Lutz, W. (2017). The human core of the shared socioeconomic pathways: Pop-  
 709 ulation scenarios by age, sex and level of education for all countries to 2100. *Global*  
 710 *Environmental Change*, *42*, 181–192. Retrieved from [http://dx.doi.org/10.1016/](http://dx.doi.org/10.1016/j.gloenvcha.2014.06.004)  
 711 [j.gloenvcha.2014.06.004](http://dx.doi.org/10.1016/j.gloenvcha.2014.06.004) doi: 10.1016/j.gloenvcha.2014.06.004
- 712 Larsen, M. A. D., Christensen, J. H., Drews, M., & Butts, M. B. (2016). Local control on pre-  
 713 cipitation in a fully coupled climate-hydrology model. *Nature Publishing Group*(April).  
 714 Retrieved from <http://dx.doi.org/10.1038/srep22927> doi: 10.1038/srep22927
- 715 Ledoux, E., Girard, G., & De Marsily, G. (1989). Spatially distributed modelling: con-  
 716 ceptual approach, coupling surface water and groundwater, in: *Unsaturated Flow in*  
 717 *Hydrologic Modeling: Theory and Practice. edited by: Morel-Seytoux, H. J.*, 435–454.
- 718 Maxwell, R. M., & Kollet, S. J. (2008). Interdependence of groundwater dynamics and  
 719 land-energy feedbacks under climate change. *Nature Geoscience*, *1*(10), 665–669. doi:  
 720 10.1038/ngeo315
- 721 Meinshausen, M., Vogel, E., Nauels, A., Lorbacher, K., Meinshausen, N., Etheridge, D. M.,  
 722 . . . Weiss, R. (2017). Historical greenhouse gas concentrations for climate modelling  
 723 (CMIP6). *Geoscientific Model Development*, *10*(5), 2057–2116. doi: 10.5194/gmd-10  
 724 -2057-2017
- 725 Meixner, T., Manning, A. H., Stonestrom, D. A., Allen, D. M., Ajami, H., Blasch, K. W.,  
 726 . . . Walvoord, M. A. (2016). Implications of projected climate change for groundwater  
 727 recharge in the western United States. *Journal of Hydrology*, *534*, 124–138. Retrieved  
 728 from <http://dx.doi.org/10.1016/j.jhydrol.2015.12.027> doi: 10.1016/j.jhydrol  
 729 .2015.12.027
- 730 O'Neill, B. C., Kriegler, E., Ebi, K. L., Kemp-Benedict, E., Riahi, K., Rothman, D. S., . . .  
 731 Solecki, W. (2017). The roads ahead: Narratives for shared socioeconomic pathways  
 732 describing world futures in the 21st century. *Global Environmental Change*, *42*, 169–  
 733 180. Retrieved from <http://dx.doi.org/10.1016/j.gloenvcha.2015.01.004> doi:  
 734 10.1016/j.gloenvcha.2015.01.004
- 735 O'Neill, B. C., Tebaldi, C., Van Vuuren, D. P., Eyring, V., Friedlingstein, P., Hurtt, G., . . .

- 736 Sanderson, B. M. (2016). The Scenario Model Intercomparison Project (ScenarioMIP)  
737 for CMIP6. *Geoscientific Model Development*, *9*(9), 3461–3482. doi: 10.5194/gmd-9-  
738 -3461-2016
- 739 Owuor, S. O., Butterbach-Bahl, K., Guzha, A. C., Rufino, M. C., Pelster, D. E., Diaz-Pines,  
740 E., & Breuer, L. (2016). Groundwater recharge rates and surface runoff response to  
741 land use and land cover changes in semi-arid environments. *Ecological Processes*, *5*(1).  
742 Retrieved from <http://dx.doi.org/10.1186/s13717-016-0060-6> doi: 10.1186/  
743 s13717-016-0060-6
- 744 Padron, R. S., Gudmundsson, L., Decharme, B., Ducharne, A., Lawrence, D. M., Mao,  
745 J., ... Seneviratne, S. I. (2020). Observed changes in dry-season water availability  
746 attributed to human-induced climate change. *Nature Geoscience*, *13*(July), 447–481.  
747 Retrieved from <http://dx.doi.org/10.1038/s41561-020-0594-1> doi: 10.1038/  
748 s41561-020-0594-1
- 749 Panda, D. K., Ambast, S. K., & Shamsudduha, M. (2021). Groundwater depletion in  
750 northern India: Impacts of the sub-regional anthropogenic land-use, socio-politics and  
751 changing climate. *Hydrological Processes*, *35*(2), 1–16. doi: 10.1002/hyp.14003
- 752 Reinecke, R., Schmied, H. M., Trautmann, T., Andersen, L. S., Burek, P., Florke, M., ...  
753 Pokhrel, Y. (2021). Uncertainty of simulated groundwater recharge at different global  
754 warming levels : a global-scale multi-model ensemble study. *Hydrology and Earth  
755 System Sciences*, *25*, 787–810.
- 756 Rodell, M., Velicogna, I., & Famiglietti, J. S. (2009). Satellite-based estimates of ground-  
757 water depletion in India. *Nature*, *460*(7258), 999–1002. Retrieved from [http://](http://dx.doi.org/10.1038/nature08238)  
758 [dx.doi.org/10.1038/nature08238](http://dx.doi.org/10.1038/nature08238) doi: 10.1038/nature08238
- 759 Roehrig, R., Beau, I., Saint-Martin, D., Alias, A., Decharme, B., Gueremy, J. F., ... Senesi,  
760 S. (2020). The CNRM Global Atmosphere Model ARPEGE-Climat 6.3: Description  
761 and Evaluation. *Journal of Advances in Modeling Earth Systems*, *12*(7), 1–53. doi:  
762 10.1029/2020MS002075
- 763 Scanlon, B. R., Faunt, C. C., Longuevergne, L., Reedy, R. C., Alley, W. M., McGuire, V. L.,  
764 & McMahon, P. B. (2012). Groundwater depletion and sustainability of irrigation  
765 in the US High Plains and Central Valley. *Proceedings of the National Academy of  
766 Sciences of the United States of America*, *109*(24), 9320–9325. doi: 10.1073/pnas  
767 .1200311109
- 768 Scanlon, B. R., Keese, K. E., Flint, A. L., Flint, L. E., Gaye, C. B., Edmunds, W. M., &  
769 Simmers, I. (2006). Global synthesis of groundwater recharge in semiarid and arid  
770 regions. *Hydrological Processes*, *20*(15), 3335–3370. doi: 10.1002/hyp.6335
- 771 SEDAC. (2018). Center for International Earth Science Information Network - CIESIN  
772 - Columbia University. 2018. Gridded Population of the World, Version 4 (GPWv4):  
773 Population Density, Revision 11. Palisades, NY: NASA Socioeconomic Data and Appli-  
774 cations Center (SEDAC). <https://doi.org/10.7927/H49C6VHW>. Accessed 18/03/21.
- 775 Seferian, R., Nabat, P., Michou, M., Saint-Martin, D., Voltaire, A., Colin, J., ... Madec,  
776 G. (2019). Evaluation of CNRM Earth System Model, CNRM-ESM2-1: Role of  
777 Earth System Processes in Present-Day and Future Climate. *Journal of Advances in  
778 Modeling Earth Systems*, *11*(12), 4182–4227. doi: 10.1029/2019MS001791
- 779 Shen, Y., Oki, T., Kanae, S., Hanasaki, N., Utsumi, N., & Kiguchi, M. (2014). Projection  
780 of future world water resources under SRES scenarios: an integrated assessment. *Hy-  
781 drological Sciences Journal*, *59*(10), 1775–1793. Retrieved from [http://dx.doi.org/  
782 10.1080/02626667.2013.862338](http://dx.doi.org/10.1080/02626667.2013.862338) doi: 10.1080/02626667.2013.862338
- 783 Siebert, S., Burke, J., Faures, J. M., Frenken, K., Hoogeveen, J., Doll, P., & Portmann,  
784 F. T. (2010). Groundwater use for irrigation - A global inventory. *Hydrology and  
785 Earth System Sciences*, *14*(10), 1863–1880. doi: 10.5194/hess-14-1863-2010
- 786 Taylor, K. E., Stouffer, R. J., & Meehl, G. A. (2012). An Overview of CMIP5 and the  
787 experiment design. *Amer. Meteor. Soc.*, *93*, 1333–1349. doi: 10.1175/BAMS-D-11-  
788 -00094.1
- 789 Taylor, R. G., Scanlon, B., Döll, P., Rodell, M., Van Beek, R., Wada, Y., ... Treidel, H.  
790 (2013). Ground water and climate change. *Nature Climate Change*, *3*(4), 322–329.

- 791 doi: 10.1038/nclimate1744
- 792 Thomas, B. F., & Famiglietti, J. S. (2019). Identifying Climate-Induced Groundwater  
793 Depletion in GRACE Observations. *Scientific Reports*, *9*(1), 1–9. Retrieved from  
794 <http://dx.doi.org/10.1038/s41598-019-40155-y>
- 795 Vergnes, J.-P. (May 2014). Développement d'une modélisation hydrologique incluant la  
796 représentation des aquifères : évaluation sur la France et à l'échelle globale. *PhD*  
797 *thesis (Institut National Polytechnique de Toulouse)*.
- 798 Vergnes, J. P., & Decharme, B. (2012). A simple groundwater scheme in the TRIP river  
799 routing model: Global off-line evaluation against GRACE terrestrial water storage  
800 estimates and observed river discharges. *Hydrology and Earth System Sciences*, *16*(10),  
801 3889–3908. doi: 10.5194/hess-16-3889-2012
- 802 Vergnes, J. P., Decharme, B., Alkama, R., Martin, E., Habets, F., & Douville, H. (2012).  
803 A simple groundwater scheme for hydrological and climate applications: Description  
804 and offline evaluation over France. *Journal of Hydrometeorology*, *13*(4), 1149–1171.  
805 doi: 10.1175/JHM-D-11-0149.1
- 806 Vergnes J.P., Decharme B, H. F. (2014). Introduction of groundwater capillary rises using  
807 subgrid spatial variability of topography into the ISBA land surface model. *Journal*  
808 *of Geophysical Research*(119), 11,065–11,086. doi: 10.1002/2014JD021573.Received
- 809 Voldoire, A., Saint-Martin, D., Senesi, S., Decharme, B., Alias, A., Chevallier, M., ...  
810 Waldman, R. (2019). Evaluation of CMIP6 DECK Experiments With CNRM-CM6-  
811 1. *Journal of Advances in Modeling Earth Systems*, *11*(7), 2177–2213. doi: 10.1029/  
812 2019MS001683
- 813 Wada, Y. (2016). Impacts of Groundwater Pumping on Regional and Global Water  
814 Resources. *Terrestrial Water Cycle and Climate Change*(May 2016), 337. doi:  
815 10.1007/978-3-319-32449-4
- 816 Wada, Y., Van Beek, L. P., Sperna Weiland, F. C., Chao, B. F., Wu, Y. H., & Bierkens,  
817 M. F. (2012). Past and future contribution of global groundwater depletion to sea-level  
818 rise. *Geophysical Research Letters*, *39*(9), 1–6. doi: 10.1029/2012GL051230
- 819 Wang, F., Ducharne, A., Cheruy, F., Lo, M. H., & Grandpeix, J. Y. (2018). Impact of  
820 a shallow groundwater table on the global water cycle in the IPSL land–atmosphere  
821 coupled model. *Climate Dynamics*, *50*, 3505–3522. Retrieved from [http://link](http://link.springer.com/10.1007/s00382-017-3820-9)  
822 [.springer.com/10.1007/s00382-017-3820-9](http://link.springer.com/10.1007/s00382-017-3820-9) doi: 10.1007/s00382-017-3820-9
- 823 Wild, M. (2012). Enlightening global dimming and brightening. *Bulletin of the American*  
824 *Meteorological Society*, *93*(1), 27–37. doi: 10.1175/BAMS-D-11-00074.1
- 825 Wilks, D. S. (2006). On 'field significance' and the False Discovery Rate. *Journal of Applied*  
826 *Meteorology and Climatology*, *45*(9), 1181–1189. doi: 10.1175/JAM2404.1
- 827 Wilks, D. S. (2016). 'The stippling shows statistically significant grid points': How research  
828 results are routinely overstated and overinterpreted, and what to do about it. *Bulletin*  
829 *of the American Meteorological Society*, *97*(12), 2263–2273. doi: 10.1175/BAMS-D-15-  
830 -00267.1
- 831 Winter, T. C., Harvey, J. W., Franke, O. L., & Alley, W. M. (1998). Ground Water and  
832 Surface Water - A single Resource - U.S. Geological Survey Circular 1139. *USGS*  
833 *Publications, Circular 1*(January 1998), 79.
- 834 Wu, W.-Y., Lo, M.-h., Wada, Y., Famiglietti, J. S., Reager, J. T., Yeh, P. J., ... Yang,  
835 Z.-L. (2020). Divergent effects of climate change on future groundwater availability in  
836 key mid-latitude aquifers. *Nature Communications*, *11*, 1–9. Retrieved from [http://](http://dx.doi.org/10.1038/s41467-020-17581-y)  
837 [dx.doi.org/10.1038/s41467-020-17581-y](http://dx.doi.org/10.1038/s41467-020-17581-y) doi: 10.1038/s41467-020-17581-y